International Journal of Concrete Structures and Materials
Vol.11, No.2, pp.215–228, June 2017
DOI 10.1007/s40069-017-0189-4
ISSN 1976-0485 / eISSN 2234-1315

Modified Disk-Shaped Compact Tension Test for Measuring Concrete Fracture Properties

Héctor Cifuentes[1),*], Miguel Lozano[2)], Táňa Holušová[3)], Fernando Medina[1)], Stanislav Seitl[3)], and Alfonso Fernández-Canteli[2)]

(Received June 16, 2016, Accepted January 31, 2017, Published online May 19, 2017)

Abstract: A new approach for measuring the specific fracture energy of concrete denoted modified disk-shaped compact tension (MDCT) test is presented. The procedure is based on previous ideas regarding the use of compact tension specimens for studying the fracture behavior of concrete but implies significant modifications of the specimen morphology in order to avoid premature failures (such as the breakage of concrete around the pulling load holes). The manufacturing and test performance is improved and simplified, enhancing the reliability of the material characterization. MDCT specimens are particularly suitable when fracture properties of already casted concrete structures are required. To evaluate the applicability of the MDCT test to estimate the size-independent specific fracture energy of concrete (G_F), the interaction between the fracture process zone of concrete and the boundary of the MDCT specimens at the end of the test is properly analyzed. Further, the experimental results of G_F obtained by MDCT tests for normal- and high-strength self-compacting concrete mixes are compared with those obtained using the well-established three-point bending test. The procedure proposed furnishes promising results, and the G_F values obtained are reliable enough for the specimen size range studied in this work.

Keywords: concrete, fracture behavior, experimental techniques, specific fracture energy, compact tension.

Abbreviations

A	Coefficient of adjustment of the tail of the P- δ or P-COD curve
a	Initial notch depth measured from load axis
A_{lig}	Ligament area
B	Specimen thickness
COD	Crack opening displacement
COD_0	Initial COD to the adjustment of the tail of the P- δ curve
COD_u	COD at the end of the test to the adjustment of the tail of the P-COD curve
CT	Compact tension
D	Depth of the notched beam
e	Notch width
E_c	Young's modulus of concrete
f_c	Compressive strength of concrete
f_{st}	Splitting tensile strength of concrete
f_t	Tensile strength of concrete
G_f	Measured RILEM specific fracture energy of concrete
G_F	Size-independent specific fracture energy of concrete
l_{ch}	Characteristic length
P	Load
$P_{\max}$	Peak load
SCC	Self-compacting concrete
W	Specimen width, i.e., distance from the load axis to the backside of the specimen
W_f	Work-of-fracture
$W_{f,m}$	Measured work-of-fracture
$W_{f,nm}$	Non-measured work-of-fracture
$W_{f,T}$	Total work-of-fracture
WS	Wedge splitting
TPB	Three-point bending
α	Relative notch length
δ	Vertical deflection at midspan
δ_0	Initial displacement to the adjustment of the tail of the P- δ curve
δ_u	Displacement at the end of the test to the adjustment of the tail of the P- δ curve
ϕ_{cs}	Outside specimen diameter
ϕ_{sb}	Pulling bar diameter

[1)]Grupo de Estructuras – ETS Ingeniería, University of Seville, 41092 Seville, Spain.
*Corresponding Author; E-mail: bulte@us.es
[2)]IEMES Research Group – EPI Gijón, University of Oviedo, 33391 Asturias, Spain.
[3)]Institute of Physics of Materials, Academy of Sciences, 616 62 Brno, Czech Republic.

1. Introduction

Compact tension (CT) tests have been widely and successfully applied for measuring the fracture properties of several materials, such as metals (ASTM Standard E399-

12E3), asphalt-aggregate mixtures (ASTM Standard D7313-13), plastics (ASTM Standard D5045-14) or even composite materials with limited orthotropy (Pinho et al. 2006). The compact tension fracture toughness test is essentially performed to propagate an initial crack by applying equal and opposite forces to the two holes previously made in the specimen through tensile clevises and pins as shown in Fig. 1. Its direct applicability in concrete, however, entails some inconveniences, such as drilling the holes necessary to apply the pulling forces and the hazard of a local fracture originated at these holes. Wittmann et al. (1988) are the pioneer in the application of CT tests in concrete but using large specimens in order to avoid premature failures. Wagoner et al. (2005), tried to apply this test methodology to smaller and disk-shaped specimens of concrete (more appropriated in case of specimens obtained from drill cores) but they ran into troubles obtaining premature failures at the pulling load holes in about 50% of the tests, thus evidencing the disability of a direct application of the procedure.

The most usual experimental procedures for measuring the specific fracture energy (G_F) of concrete (Karihaloo 1995) avoiding the problems associated with the CT tests are the three-point bending test (TPB) and the wedge splitting test (WS). The former, carried out on prismatic notched beams, is the most widespread procedure due to its simplicity and the satisfactory results it provides (Abdalla and Karihaloo 2003; Bazant 1996; Bazant and Kazemi 1991; RILEM 1985). The latter requires notched compact specimens, usually cube or prismatic specimens, preventing the mentioned disadvantages of the conventional CT specimens

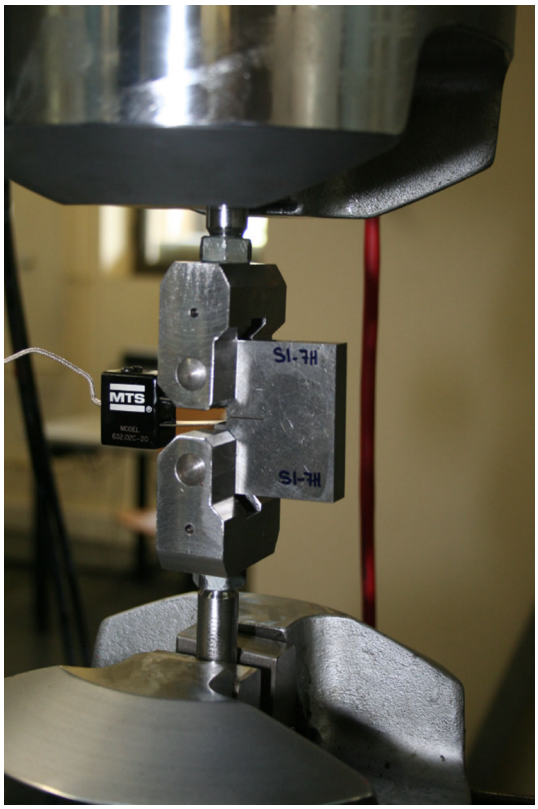

Fig. 1 Round compact tensile test specimen and tensile clevises and pins.

(Bruhwiler and Wittmann 1990; Cifuentes and Karihaloo 2013; Wittmann et al. 1988).

However, when the mechanical and fracture behavior of a concrete in an already built structure is required, cylindrical drilled cores are extracted from the concrete structure allowing the compressive strength, the splitting tensile strength and the Young's modulus of concrete to be easily determined (Abou El-Mal et al. 2015; Harkouss and Hamad 2015). In this case, the CT test seems to be the suitable test for measurement of the specific fracture energy by using slice shaped specimens cut off from the cylindrical cores, in particular if the above mentioned disadvantages in testing such specimen type are surmounted.

In spite of the CT test method being proposed by a RILEM recommendation (RILEM 1985), only few papers in the literature are related to the use of such a test for measuring the specific fracture energy of concrete, most of them being referred to specimens with rectangular shape as extracted from cubic compression specimens (Issa et al. 2000; Pandey et al. 2016; Van Mier 1991). The utilization of disk-shaped compact tension (DCT) specimen geometry is common for the analysis of fracture energy by asphalt materials (Kim et al. 2009; Wagnoner et al. 2005; Wagoner et al. 2006; Zofka and Braham 2009), whereas its use by plain concrete is very limited (Amirkhanian et al. 2011, 2016) mainly due to the mentioned premature failures originated at the surrounding edge of the pulling holes.

This work promotes the applicability of the so-called *modified* disk-shaped compact tension (MDCT) test, as an alternative and reliable pulling solution to the conventional CT or DCT, using also cylindrical shape specimens for measuring the specific fracture energy of concrete, in particular when the fracture behavior of a concrete in an already built structure must be assessed. Basically, the new procedure consists in applying the pulling force by means of reinforced bars already built in the specimen, either already by the specimen concrete casting or by subsequent boring and gluing, which are clamped in the machine during testing (Nieto et al. 2014). In this way, outfitting holes in the specimen is avoided thus lowering the ratio of invalid tests, due to the local fracture in the pulling holes, practically to nil.

In the following, a description of the proposed method, its geometry, the way to prepare the specimens and the test set up is thoroughly detailed. Additionally, an experimental investigation is carried out to evaluate the applicability of the method. MDCT tests are performed according to the work-of-fracture method for two different self-compacting concrete (SCC) mixes (normal- and high-strength concrete). The size of the specimen ligament area is varied in order to check the size independency of the specific fracture energy obtained. The results are compared with those obtained by applying the well validated TPB tests, leading to the conclusion that the proposed modified compact tension method is accurate enough to estimate the specific fracture energy of concrete in a simple way, representing an optimal alternative for it to be applied in case of an existing concrete structure. It should be noted that this MDCT tests can also be applied for

determining other additional fracture parameters, such us the stress intensity factor or the critical mouth opening displacement of concrete. Nevertheless, these parameters are related with equivalent linear-elastic fracture models and this work is focused on applicability of the fictitious crack model.

2. Background: Determination of the Size-Independent Specific Fracture Energy of Concrete

2.1 Work-of-Fracture Method

The work-of-fracture method was developed by Hillerborg et al. (1976) for experimental determination of the specific fracture energy in concrete The method, based on the fictitious crack model, is included in a RILEM Standard Recommendation (RILEM 1985) for measuring the fracture energy of concrete, G_f. According to this method, the specific fracture energy of concrete (energy per unit area necessary to break the concrete) is obtained as follows:

$$G_f = \frac{W_f}{A_{lig}} \tag{1}$$

where W_f is the work-of-fracture supplied by the external load (machine) and A_{lig} is the ligament area of the specimen.

Although the main work-of-fracture test methods traditionally applied to concrete are the TPB and the WS tests due to their simplicity and their ability of complying with the main hypothesis required, different kind of tests can be proposed provided the external work can be easily measured, the ligament area is localized, the cracking is only caused due to tensile stresses and no energy dissipation takes place outside the ligament area. All of these tests must have in common their requirement of being applied on notched specimens in order to guarantee the crack propagation being localized in the ligament area.

The TPB test (Fig. 2a) is the most widely method used for concrete fracture analysis due to the simple specimen preparation and execution (Abdalla and Karihaloo 2003; Bazant 1996; Bazant and Kazemi 1991; RILEM 1985), even for fiber-reinforced concrete (Cifuentes et al. 2013; Gopalaratnam and Shah 1987). However, the correct execution of the TPB method is not exempted of complications requiring some important aspects as to avoid energy dissipations outside the ligament area and to reduce the influence of the specimen geometry and loading type on the results. Firstly, the supports and the tool employed for the transmission of the vertical load to the beam have to be properly designed. Further, the measuring system should be fixed to the beam to avoid unrealistic vertical deflection measurements caused by the torsional free-twist of the beam. According to this, consideration of the vertical displacement of the hydraulic actuator as the measurement of the vertical deflection is not correct and a linear variable differential transformer (LVDT) transducer has to be mounted on a reference frame (Karihaloo 1995). Lastly, the specimen self-

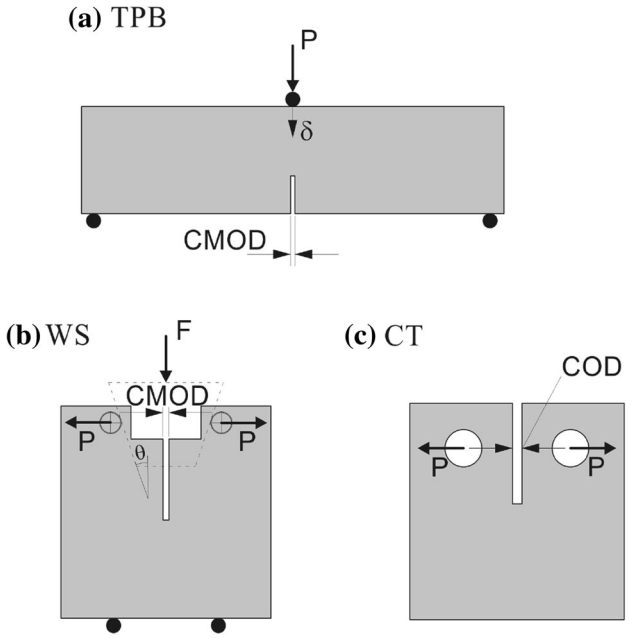

Fig. 2 Schematic representation of several usual tests for measuring the specific fracture energy of concrete. **a** Three-point bending, **b** wedge splitting and **c** compact tension specimens.

weight, as influencing the experimental results, must be compensated or taken into account for a correct determination of the work-of-fracture during the test. As an example, Guinea et al. propose the utilization of elastomeric springs to avoid tensile stresses in the ligament area due to the self-weight (Guinea et al. 1992).

Once the P–δ curve is recorded for each specimen tested, the work-of-fracture is determined as:

$$W_f = \int_0^{\delta_u} P d\delta \tag{2}$$

where δ_u is the vertical deflection at the end of the test.

The WS test (Fig. 2b), as developed by Linsbauer and Tschegg (1986) was subsequently modified by Bruhwiler and Wittmann (1990) proving to be a very stable test for determining the fracture energy of concrete. The specimens used in this method are fairly compact requiring small amounts of material as compared with the notched beams employed in three-point bending tests. However, the implementation of this test type requires a more sophisticated fixture than that implied by the three-point bending test so that the number of results available in the literature from WS tests for concrete is scarce (Cifuentes and Karihaloo 2013; Korte et al. 2014; Merta and Tschegg 2013; Veselý et al. 2011). The fracture behavior is analyzed by wedging out the starter notch. The testing has to be carried out using a closed-loop testing machine and under displacement control at a very low rate so that the specimen fracture occurs in a stable manner (Abdalla and Karihaloo 2003; Cifuentes and Karihaloo 2013). Since the direct application of two pulling forces to stable split of the specimen entails a great difficulty,

the usual loading arrangement consists in a wedge made from steel that is mounted between two bearings, which transform the vertical applied load (F) into two horizontal splitting loads (P) (Cifuentes and Karihaloo 2013). Additionally, the specimen is usually placed on a linear support (steel rod) fixed to the lower plate of the testing machine. Some researchers have proposed placing two linear supports in order to eliminate the weight effect of the specimens (Abdalla and Karihaloo 2003). If bearing friction is neglected, the splitting load can be calculated as:

$$P = \frac{F}{2\tan\theta} \tag{3}$$

where θ is one-half of the wedge angle (Fig. 2b). According to this, an equivalent *P-CMOD* curve can be obtained from the recorded *F-CMOD* curve for each specimen tested, so that the work-of-fracture is calculated as follows:

$$W_f = \int_0^{CMOD_u} PdCMOD \tag{4}$$

where $CMOD_u$, is in this case the crack mouth opening displacement at the test completion.

In metallic materials, testing CT specimens represents a usual procedure to determine fracture parameters, whereby ASTM Standard E-399 specifies the geometry and general configuration of this kind of tests. In such CT tests (Fig. 2c) an eccentric tensile force has to be applied on the ligament area of a previously notched sliced specimen with circular or rectangular geometry. The crack opening displacement of the notch lips at the level of the axis load must be recorded. In this way, the load-*COD* (*P-COD*) curve is obtained and the work-of-fracture is directly obtained as the area under the curve. The tools necessary to perform the conventional CT tests on concrete are difficult to be designed and their implementation is not as easy as in case of the TPB test.

2.2 Size Dependency of the Specific Fracture Energy of Concrete

The values determined by the work-of-fracture method as proposed in RILEM recommendation (RILEM 1985) are dependent on the specimen size and shape used in the test, as demonstrated and analyzed by several researchers in the past (Hu and Wittmann 1992; Kwon et al. 2008; Muralidhara et al. 2011; RILEM 2004; Vydra et al. 2012). The two most popular models to obtain a size-independent specific fracture energy of concrete (also called true fracture energy (Karihaloo et al. 2003)) are the boundary effect model of Hu and Wittmann (1992) and the experimental correction model to avoid energy dissipations proposed by Guinea et al. (Elices et al. 1992; Guinea et al. 1992; Planas et al. 1992). Although these models are based on different fundamentals, they are related to each other. Cifuentes et al. (2013) showed that if the size-dependent G_f measured by the RILEM method is corrected according to the method of Elices and co-workers (Elices et al. 1992; Guinea et al. 1992; Planas et al. 1992) or that of Hu and Wittmann (1992) (the latter admits a simplification as proposed by Karihaloo et al. (2003) if the notch to depth ratios are well apart from each other), then the resulting specific fracture energy G_F is very nearly the same and independent of the size of the specimen.

The methodology of Hu and Wittmann (1992), based on the local fracture energy concept as thoroughly detailed in several papers (Cifuentes and Karihaloo 2013; Hu and Wittmann 1992), states that the size effect on G_f (measured specific fracture energy according to work-of-fracture method) is caused by a variation of the fracture process zone when the crack approaches the free boundary surface of the specimen at test completion (Hu and Wittmann 1992). On the other hand, among the several sources of experimental errors analyzed by Guinea et al., the most significant proves to be the influence of the non-measured fracture energy of concrete due to the curtailment of the upper tail of the P–δ curve (Elices et al. 1992). Accordingly, the methodology proposed by Guinea and co-workers (Elices et al. 1992; Guinea et al. 1992; Planas et al. 1992) involves adding the non-measured work-of-fracture due to the curtailment of the tail of the load-central deflection (P–δ) curve recorded in the three-point bend test.

Guinea et al. demonstrate that the non-measured work-of-fracture ($W_{f\cdot nm}$) for a three-point bending test of a notched beam with compensated self-weight, can be determined by extrapolating the upper tail of the P–δ curve beyond the limits of the recorded test results using the expression:

$$W_{f\cdot nm} = \int_{\delta_u}^{\infty} Pd\delta = \frac{A}{\delta_u} \tag{5}$$

where A is the fitting experimental coefficient of the tail of the P'–δ curve between δ_0 and δ_u. δ_0 is usually considered as the vertical displacement corresponding to a load of 5% of the peak load ($P_{\max}$) (Lee and Lopez 2014; RILEM 2007) and δ_u is the last recorded mid-span deflection of the specimen at the end of the test (Fig. 3). Once the non-measured work-of-fracture is estimated, the size-independent fracture energy of concrete is obtained as (Elices et al. 1992):

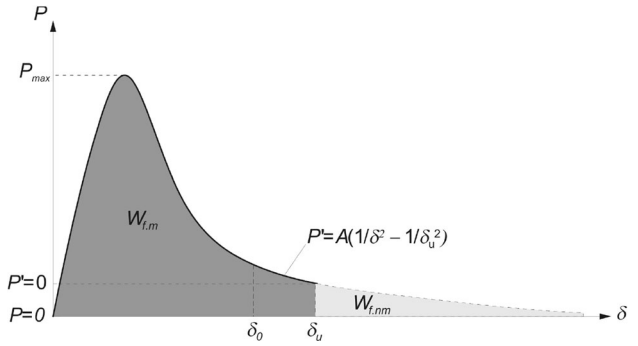

Fig. 3 P–δ curve for a three-point bend test showing the measured (W_f) and non-measured ($W_{f\cdot nm}$) work-of-fracture.

$$G_F = \frac{\int_0^{\delta_u} P d\delta + A/\delta_u}{B(D - a_0)} \tag{6}$$

where G_F denotes a size-independent value of the specific fracture energy.

3. Description of the MCT Specimens and Test

The MDCT specimens are based on the conventional DCT test concept relative to a notched specimen with cylindrical shape (Nieto et al. 2014), allowing the pulling force to be applied in a simple way without the inconvenience of possible material local fractures at the pulling holes due to stress concentration, as would happen by conventional DCT concrete specimens. Initially, the modified disk-shaped compact tension test solution included sliced shape specimens cut off from cylindrical specimens as used in standard compression tests or from drill cores as extracted from real constructions for evaluating age and conditions of the material. In such a case, the pulling bars must be allocated and glued (e.g. by using epoxy resin) into the holes drilled out into the specimens in transversal direction to the notch milled, as shown in Fig. 4. In the meantime, more simple and practical solutions, here denoted "ad-hoc" specimens, are developed to facilitate their preparation in the laboratory. In both MDCT solutions, i.e. "drill-out" and "ad-hoc" specimens, the geometry is apparently the same, consisting in notched cylinders of a suitable thickness, B, furnished with the pulling bars, as shown in Fig. 4, though requiring two different manufacturing procedures. In this work "ad-hoc" specimens are studied. ϕ_{cs} is the outside specimen diameter, ϕ_{sb} is the pulling bar diameter, a is the initial notch depth measured from load axis, B is the specimen thickness, e is the notch width, A_{lig} is the ligament area, and α is the relative notch length.

From these values, the ligament as the area of specimen to be fractured, is calculated as the product of the length of the ligament times the thickness of the specimen, see Eq. (7). On its turn, the dimensionless relative notch length α as defined in Eq. (8), is considered the reference parameter to be studied in the modified compact tension tests of concrete, the same as in the original compact tension tests (Harkouss and Hamad 2015).

$$A_{lig} = B(W - a) \tag{7}$$

$$\alpha = a/W \tag{8}$$

Once the specimens are prepared, the execution of the test is very simple using a universal machine equipped with two clamps vertically aligned. This machine and the fixtures needed are usually available in standard laboratories. The procedure consists in clamping one of the ends of the pulling bar to the lower grips, which stay fixed, while the other bar is clamped to the upper grips, which move vertically up transmitting the load to the specimen. Thus, as the displacement of the upper grips increases, a crack is generated in the specimen starting at the notch tip until achieving the complete rupture of the specimen. Tests must be performed by displacement control of the machine and the crack opening displacement in the notch lips at the level of the alignment of the pulling bars (COD) should be controlled and recorded. Then, the P-COD curve is obtained and the work-of-fracture, W_f, determined in a similar way as in the TPB and WS tests as the area under the P-COD curve. The specific fracture energy of concrete (probably size-dependent), G_f, is then given by:

$$G_f = \frac{\int_0^{COD_u} P dCOD}{A_{lig}} \tag{9}$$

where COD_u is the crack opening displacement at the test completion. In this case, the load directly applied by the testing machine is the load that produces the crack opening without the need of any further transformation, as in case of the original CT or DCT test. It should be noted that the crack mouth opening displacement (CMOD) can be also measured and the test can be alternatively controlled by this value. Nevertheless, according to the procedure herein described measurement of the CMOD is not necessary and the clip gauge transducer can be located at the notch lips and aligned with the steel bar axis to measure the COD.

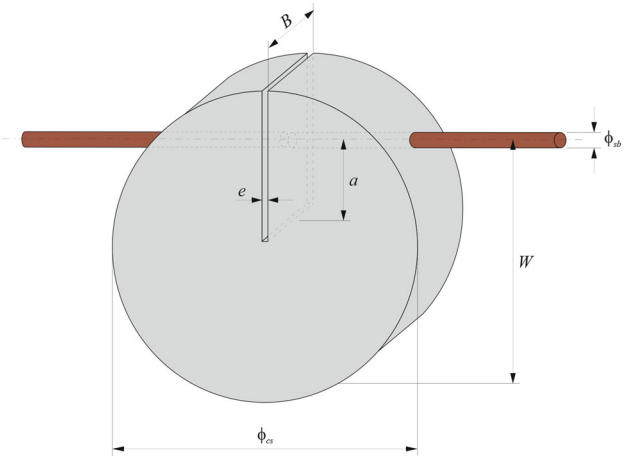

Fig. 4 Characteristic geometry of the MCT specimens.

4. Experimental Program

In order to confirm the applicability of the MDCT test for measuring the specific fracture energy of concrete, a comprehensive experimental investigation is carried out. Several geometry configurations of the MDCT specimens with varying size of the ligament area are tested in order to study the influence of the specimen geometry on the results. Moreover, TPB tests are also performed to obtain a reference size-independent value of the specific fracture energy of concrete G_F with the aim of comparing and verifying the results from the MDCT tests.

Table 1 Constituents and mix proportions for normal- and high-strength self-compacting concrete mixes.

Constituents (kg/m^3)	NSC	HSC
Cement	376	500
Micro-silica	–	75
Coarse aggregates (crushed limestone) < 10 mm	580	990
Sand < 2 mm	739	660
Water	192	134
Limestone powder (<2 mm)	545	105
Super-plasticizer (SIKA Viscocrete 20HE)	3.0	18.4
Water/cement	0.51	0.23
Flow spread (mm)	710	695
T_{500} (s)	3.1	3.4

4.1 Materials

Both tests, MDCT and TPB, are performed for the same concrete mixes. To extend the validity of the results, two different self-compacting concrete mixes are designed. One of the mixes is made of normal-strength concrete (NSC) and the other mix, of high-strength concrete (HSC). In both cases, an ordinary Portland cement CEMII/B-V 32.5R is used with 10 mm maximum aggregate size. Their target cube compressive strengths are 40 and 100 MPa, respectively. The mix proportions and constituents are shown in Table 1. In case of HSC mixes micro-silica has been used to densified the concrete matrix.

The characteristic compressive strength (f_c) is determined from 100 mm^3 cubes in accordance with UNE EN12930-3:2009. The indirect tensile strength (f_{st}) is obtained from splitting tests (Brazilian tests) using 100 mm diameter by 200 mm long cylinders, according to UNE EN12930-6:2010. The static elastic modulus of concrete (E_c) is determined according to the UNE EN12390-13:2014 by gradually loading a cylindrical specimen in compression to approximately a third of its failure load and measuring the corresponding strain from 30 mm strain gauges. The values of the mean and coefficient of variation measured for the mechanical properties of both concrete mixes are given in Table 2.

4.2 Modified Disk-Shaped Compact Tension Tests

In this study, "ad hoc" MDCT rather than "drilled out" specimens are prepared for being tested in the laboratory, allowing the same concrete to be employed in both MDCT and TPB tests and the results to be conveniently compared.

The procedure of manufacturing of the MDCT specimens is fairly simple. In order to obtain cylindrical shape specimens, a PVC pipe with internal diameter of 153 mm is taken as a mold, the outside diameter of specimens being determined by this value (Fig. 5a). Next, the pulling steel bars, which will be embedded in the concrete mass after casting, are threaded through the molds at the prescribed position, W, for the prospective specimen axis with respect to the ligament back side, and at regular vertical axial distances. Usual corrugated steel bars with 8 mm in diameter are advantageously employed (Fig. 5b). At this time, the concrete mixes are poured into the molds and cured in a water tank during 28 days. Thereafter, sliced shape specimens of 60 mm thickness are cut off from the cylindrical molds so that the steel bars remain in the mid-plane of the specimen (Fig. 5c). To diminish the effect of segregation of aggregates because of the height of the cylinder molds and the presence of the steel bars, the bottom part of the filled cylinders is not considered in obtaining the samples and specimens are obtained from the central part of the cylinders. Lastly, the notch is mechanized according to the prescribed notch depth chosen (Fig. 5d). The final outlook of the notched sliced specimens is shown in Fig. 6. In Table 3 the dimensions of the different MDCT specimens tested are shown whereby two different distances from the load axis (axis of the steel pulling bars) to the ligament back side of the specimen and three different relative notch depths are chosen. In that way, six different sizes of the ligament area are tested for each concrete mix and the influence of the specimen geometry

Table 2 Mechanical properties of NSC and HSC concrete mixes.

Concrete	F_c (MPa)	F_{st} (MPa)	E_c (GPa)
NSC	36.8 ± 2%	3.8 ± 9%	24.4 ± 4%
HSC	97.0 ± 3%	5.7 ± 4%	41.3 ± 3%

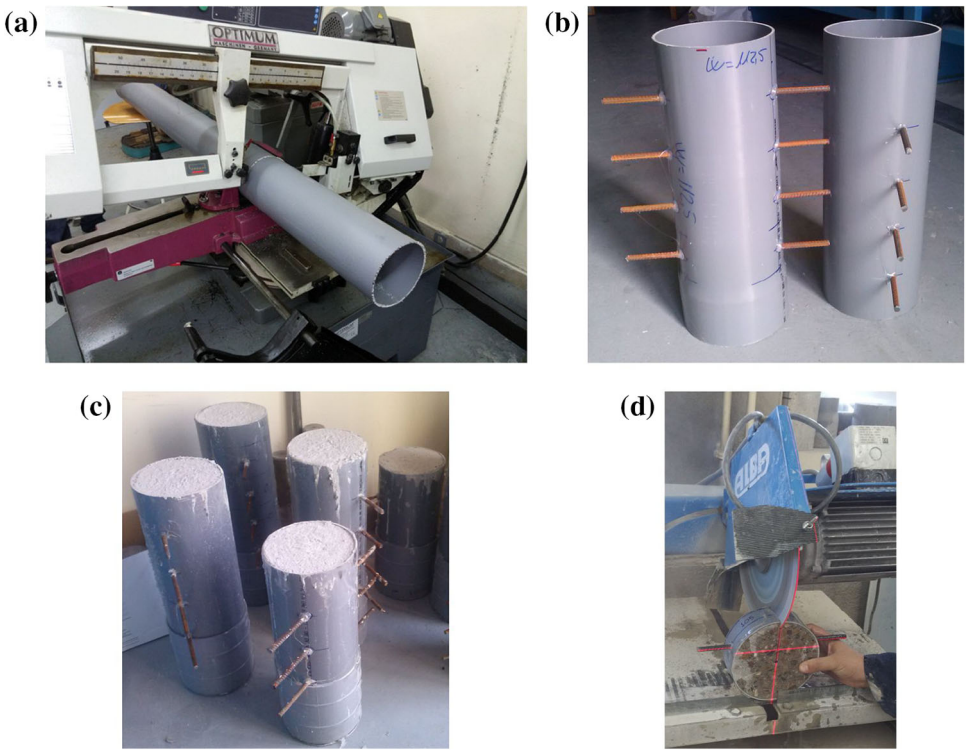

Fig. 5 Preparation of MDCT specimens. **a** Sawing PVC pipe tube. **b** Threaded pulling bars at regular distances. **c** Molds with casted concrete. **d** Mechanizing the notch.

can be analyzed. As stated by different researchers, the size effect on fracture energy can be accurately analyzed by varying the relative notch depth (Cifuentes and Karihaloo 2013; Hu and Wittmann 1992). In this case, even if the outside diameter of specimen remains the same, a variation in the position of the axis of the steel pulling bars allows the effective height (size) of the specimens to be varied. It should be noted that the dimension of the outside diameter of the specimen, in this case 153 mm, practically coincides with that of the standard cylinder specimen used for compressive strength determination and remains in the same order of magnitude as the depth of 100 mm commonly exhibited by the prismatic used for the G_F determination in the case of TPB tests.

All tests are carried out in a servohydraulic test machine MTS Bionix with 25 kN of load capacity, see Fig. 7. Tests are performed under displacement control of the machine with a rate of 0.2 mm/min. All deformations and displacements of the specimens during the tests are measured by a 3-D digital image correlation equipment ARAMIS of GOM. This technique is successfully used by different researchers to study cracking and fracture behavior of concrete (De Wilder et al. 2016; Nam and Lee 2015; Shah and Kishen 2011). Alternatively, a clip gauge transducer located at the notch lips and aligned with the steel bar axis could be additionally used. In that way, the full load-*COD* (*P*-*COD*) curves for all specimens would be obtained after post-processing of the digital images recorded during the test. Accurate determination of such a load-*COD* is crucial for assessing the work-of-fracture applied to split the specimen into two halves.

4.3 Three-Point Bending Tests

With the aim of comparing the MDCT test results with those using standard procedures, three-point bend tests with prismatic notched specimens are performed according to the experimental requirements of the work-of-fracture method described in the RILEM recommendation (RILEM 1985). The size-independent value of the specific fracture energy G_F is determined according to the procedure proposed by Guinea et al. (Elices et al. 1992; Guinea et al. 1992; Planas et al. 1992). Table 4 shows the geometrical dimensions of the specimens as displayed in Fig. 8.

Four samples are tested for each mix of concrete, from whose results the mean value and the coefficient of variation for every analyzed parameter are obtained. The initial tangent correction due to crushing of concrete at the supports is applied for all specimens. Three-point bending tests are performed with the indicated self-weight compensation. All tests are carried out in a closed-loop servo-hydraulic dynamic 25 kN MTS Bionix testing machine. The rate of loading is controlled by a crack mouth opening displacement (*CMOD*) gauge at a very low rate (0.001 mm/s) so that the fracture occurs in a stable manner. The *CMOD* displacement is measured with a clip gauge transducer whereas a LVDT linear displacement transducer, fixed to the bottom of the specimen by means of a reference frame, is used to measure the vertical displacement at the midpoint (Fig. 9). The load-*CMOD* (*P*-*CMOD*) and load–displacement (P-δ) curves are recorded for all specimens. The test interruption is decided as a function of the last displacement value being obtained by the fracture curve for any of these specimens.

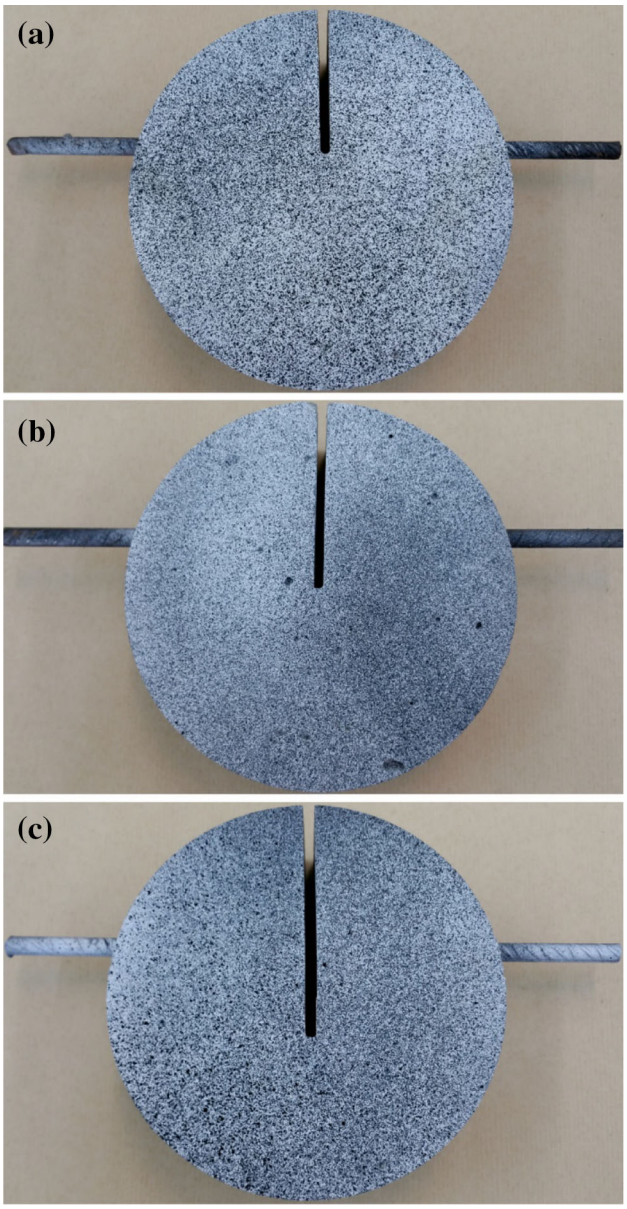

Fig. 6 Final outlook of the MDCT specimens for different notch depths: **a** $\alpha = 0.1$, **b** $\alpha = 0.3$ and **c** $\alpha = 0.5$.

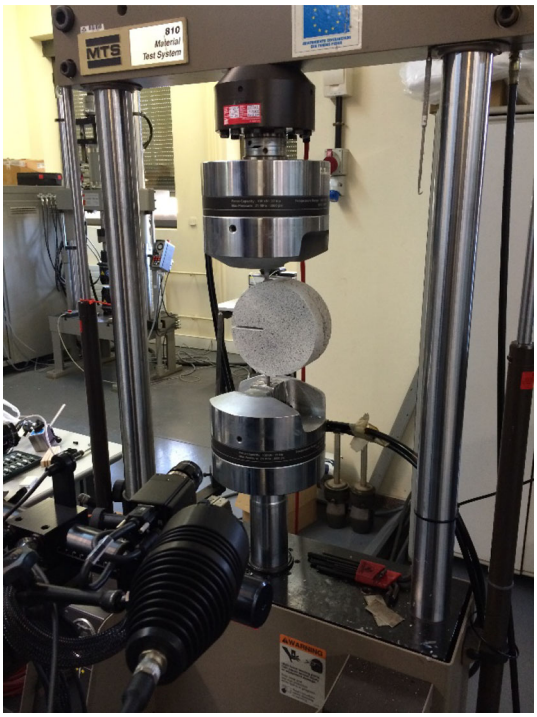

Fig. 7 MDCT test of a cylindrical sliced shape specimen with $\alpha = 0.1$.

5. Results

5.1 MDCT Tests

The recorded *P-COD* curves obtained from the MDCT tests carried out for the different geometries, as indicated in Table 3, are shown in Fig. 10. Although four samples of each relative notch depth are tested, only one representative curve is just represented for each α in order to facilitate an overview of the graphs.

Sometimes, due to the pulling bars stiffness and their rigid build into the concrete, an affected part of the load-COD curve may be observed at the upper tail of the curve when the crack is approaching the ligament back free boundary (see Fig. 10). At the test beginning, the crack opening displacement necessary to break the concrete is relatively low so that the moments arising by bending of the pulling bars are negligible. Nevertheless, as the test progresses and the necessary COD to further opening of the crack increases, the pulling bar-concrete interaction acts against crack propagation. As a result of such phenomenon, the observed behavior evidences in the most cases a very long tail trending to a constant value of the load, which does not tend asymptotically to zero while in some few cases, an increase of the load can be even observed. However, the fracture process of the concrete seems to happen correctly as the crack path always runs in perpendicular direction to the loading axis. Some

Table 3 Dimensions of the MDCT specimens tested in the experimental program.

Specimen	MCT1	MCT2
ϕ_{cs} (mm)	153	153
ϕ_{sb} (mm)	8	8
W (mm)	112.5	105
b (mm)	60	60
e (mm)	4	4
α	0.1–0.3–0.5	0.1–0.3–0.5

Table 4 Geometrical parameter values of notched beams used in TPB tests.

Specimen	D (mm)	B (mm)	S (mm)	L (mm)	A (mm)	S/D	$\alpha = a/D$
TPB	100	100	400	440	50	4	0.5

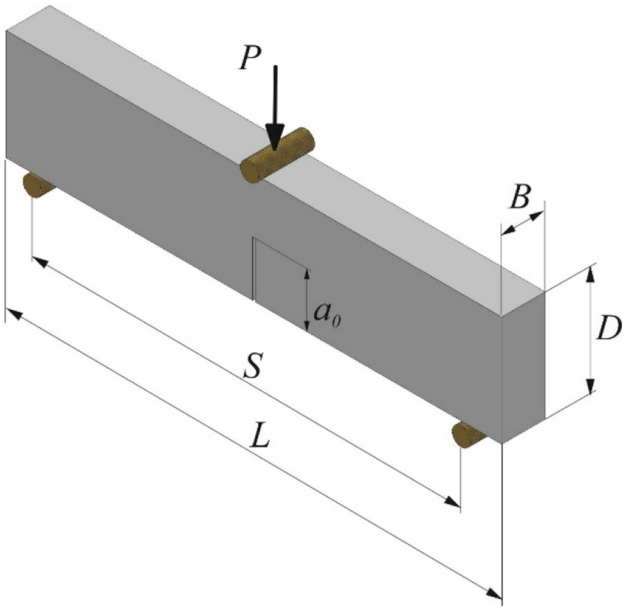

Fig. 8 Geometrical shape parameters of notched specimens used in the TPB tests.

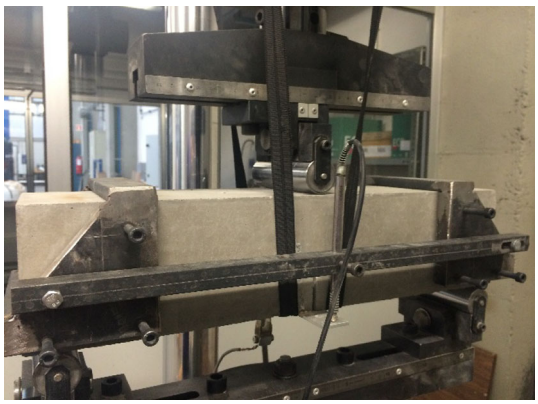

Fig. 9 Three-point bend test of prismatic notched specimens with weight compensation.

images of the crack propagation as captured by the 3D Aramis equipment during one of the MDCT tests are shown in Fig. 11. As can be observed, the crack propagation path is that being expected for this kind of test and the opening mode corresponds to pure mode I.

In order to amend this discordant behavior at the tail of the curve, i.e. the end of the test, a curve processing, based on the adjustment of the tail proposed by Guinea et al. in case of TPB tests, is proposed. The *P-COD* curve corresponding to a NSC-MDCT test with height $W = 112.5$ mm and relative notch depth $\alpha = 0.5$ is shown in Fig. 12a exhibiting, both in the ascending part but also at the most part of the descending branch until a certain small value of the load, a typical shape as expected from the work-of-fracture method, while close to the end of the test the curve behavior becomes affected. The proposal suggests removing the affected part for each of the specimens tested what implies part of the *P-COD* curve not being included as an area under the curve contributing to the total work-of-fracture being involved in the concrete fracture of the ligament. Accordingly, this area should be estimated in order to obtain this non-measured work-of-fracture as explained by Guinea et al. for TPB tests (Kwon et al. 2008). The same concept can be here applied once the tail of the remaining curve is fitted using the following expression:

$$P' = A\left(\frac{1}{COD^2} - \frac{1}{COD_u^2}\right) \tag{10}$$

where $P' = 0$ for COD_u. The non-measured work-of-fracture can be estimated as:

$$W_{f,nm} = \frac{A}{COD_u} \tag{11}$$

According to Fig. 11b, the COD_0 is the initial crack opening displacement considered for fitting the tail of the curve, COD_u is the ultimate crack opening displacement until the *P-COD* is found to be correct and A is the coefficient for fitting the tail of the curve between COD_0 and COD_u as shown in Fig. 11b.Once the curve is amended, the measured work-of-fracture is given by:

$$W_{f,m} = \int_0^{COD_u} PdCOD \tag{12}$$

which represents the area under the *P-COD* curve until the COD_u value. The size-independent specific fracture energy of concrete can be now determined as follows:

$$G_F = \frac{W_{f,nm} + W_{f,m}}{B(W - a)} \tag{13}$$

Assuming the proposal is correct, its applicability can be checked by comparing the specific fracture energy of concrete just obtained with that from the TPB tests since the concrete mixes for MDCT and TPB tests are the same and no variation due to the material is expected.

Table 5 shows the main results necessary to calculate the specific fracture energy of concrete according to the work-of-fracture method applied to MDCT specimens, where COD_0 is the crack opening displacement at the level of the loading axis considered for fitting the *P-COD* curve, COD_u is the ultimate crack opening displacement considered to avoid the affected part of the curve at the end of the test, A is the coefficient for fitting the tail of the *P-COD* curve, $W_{f,nm}$ is the non-measured work-of-fracture as indicated in

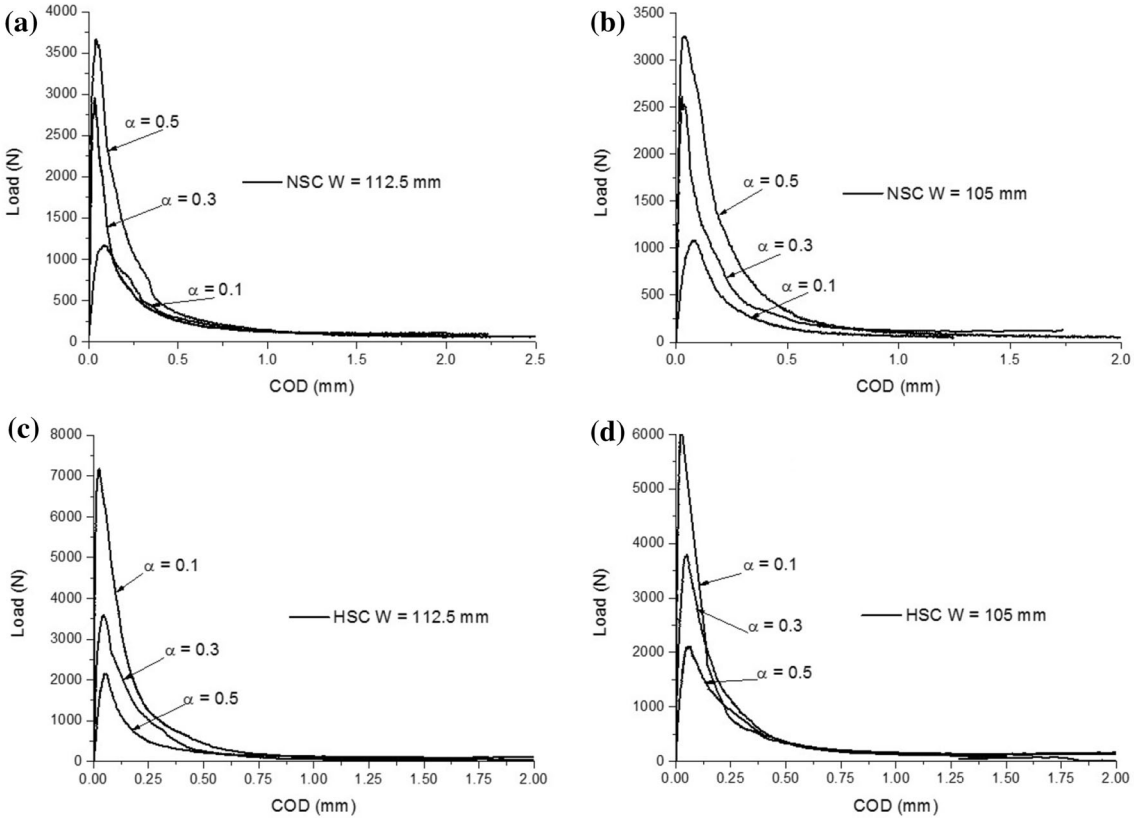

Fig. 10 Load-COD curves obtained from MDCT tests: **a**, **b** for normal-strength concrete and **c**, **d** for high-strength concrete.

Eq. (12), $W_{f,m}$ is the measured work-of-fracture under the *P-COD* curve, $W_{f,T}$ is the total work-of-fracture, A_{lig} is the ligament area of the different specimens and G_F is the size-independent specific fracture energy of concrete.

The values considered for COD_u in this work are those corresponding to a load of about the 15% of the peak load in the softening branch of the *P-COD* diagram. In case of COD_0, the values adopted are $0.55COD_u$ approximately.

As may be observed in the results shown in Table 5, the values of the specific fracture energy of concrete obtained as indicated above (i.e. fitting the tail of the curve after eliminating the affected part of the curve due to the interaction between pulling bar and concrete) are roughly the same, independently of the relative notch depth and height of the pulling bars. In case of NS concrete, the minimum mean obtained value is 155.2 N/m for $W = 112.5$ mm and $\alpha = 0.3$ and the maximum obtained value is 164.4 N/m for $W = 112.5$ mm and $\alpha = 0.5$. The maximum coefficient of variation of results is 15%, which means that values of G_F obtained for the different NSC-MDCT tests are statistically the same. A similar analysis, with the same conclusion, can be made for the HSC-MDCT test results. In that way, according to the proposed procedure, the G_F values obtained are not dependent of the specimen geometry in the range of the sizes tested, as required for a parameter to be considered as a material property. It should be noted, that to reduce the effect of the rigid union between steel bars and concrete on the tail of the behavior curve of concrete another fixture system, allowing the rotation between the pulling bars and concrete, could be also employed.

5.2 TPB Tests

In Table 6, the mean value and the coefficient of variation of the material parameters corresponding to both mixes of concrete used to obtain the specific fracture energy of concrete are presented, where m is the mass of the specimen, δ_0, the initial value of the displacement considered by fitting the tail of the curve, δ_u, the displacement when the test is stopped, $W_{f,m}$, the measured work-of-fracture under the load–displacement curve, A, the coefficient of fitting the upper tail of the curve, $W_{f,nm}$, the non-measured work-of-fracture according to Eq. (11), A_{lig}, the real ligament area measured in the specimens, and G_F, the specific fracture energy of concrete, which is size-independent according to Guinea et al.

This procedure is repeatedly validated by different researchers, and the value of G_F so determined is demonstrated to be correct and claimed as being the size-independent specific fracture energy of concrete.

6. Analysis of Results

Table 7 summarizes the G_F results obtained for the two different concrete mixes studied in the present work using

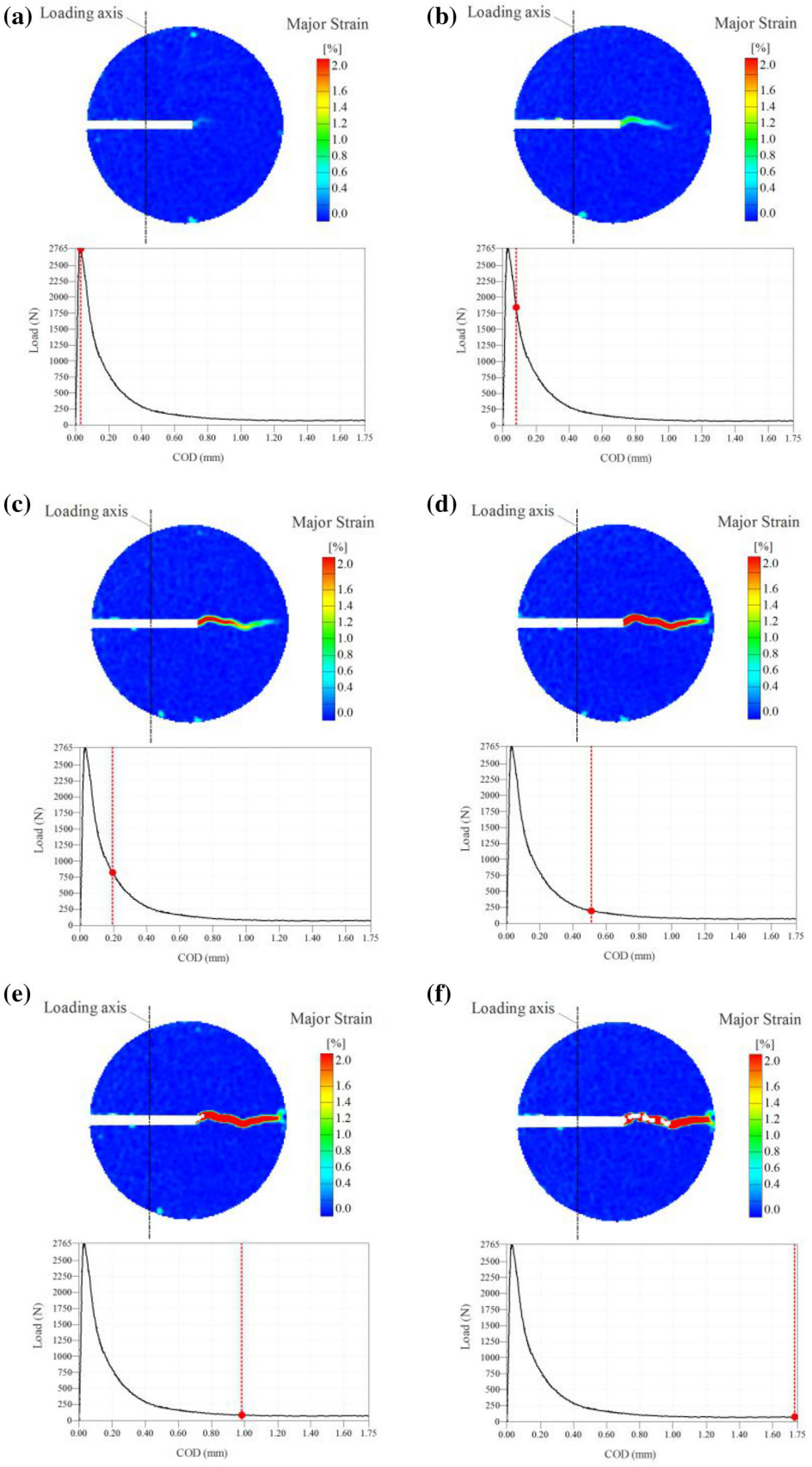

Fig. 11 **a–f** Crack path evolution during the MDCT test for one of the specimens tested.

the TPB and MDCT tests. In case of MDCT test, the result represents the mean value obtained for the different heights W and relative notch depths α considered in this work.

As can be seen, the results from the MCT tests are slightly higher than those from TPB (less than 7% in the worst case). This can be attributed to the bending stiffness of the steel

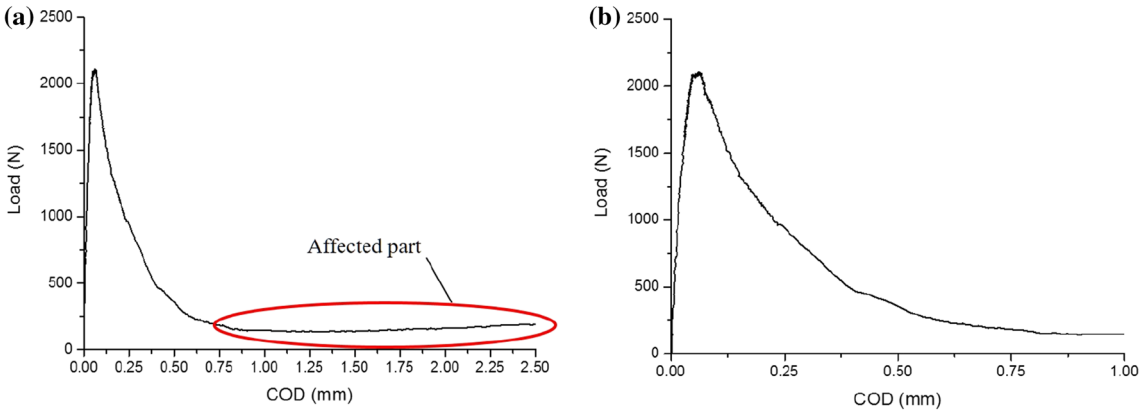

Fig. 12 **a** *P-COD* curve corresponding to the MDCT test for $W = 112.5$ mm and $\alpha = 0.5$. **b** Proposed tail fitting for the *P-COD* curve after removing the affected part.

Table 5 Results from MDCT tests.

Concrete	W (mm)	α	COD_0 (mm)	COD_u (mm)	A (Nmm^2)	$W_{f,NM}$ (Nmm)	$W_{f,M}$ (Nmm)	$W_{f,T}$ (Nmm)	A_{lig} (mm^2)	G_F (N/m)
NSC–MDCT	105	0.1	0.67	1.25	61 ± 14%	49 ± 13%	557 ± 18%	607 ± 16%	3748 ± 1%	161.9 ± 3%
		0.3	0.50	0.96	39 ± 11%	41 ± 14%	689 ± 15%	730 ± 15%	4528 ± 1%	161.4 ± 15%
		0.5	0.75	1.50	104 ± 8%	70 ± 19%	934 ± 8%	1004 ± 11%	6177 ± 1%	162.6 ± 5%
	112.5	0.1	0.75	1.25	79 ± 15%	52 ± 12%	498 ± 12%	550 ± 11%	3343 ± 1%	164.0 ± 11%
		0.3	0.50	0.80	48 ± 14%	66 ± 4%	712 ± 13%	778 ± 13%	5014 ± 1%	155.2 ± 13%
		0.5	0.60	1.50	59 ± 9%	53 ± 14%	895 ± 14%	948 ± 15%	5767 ± 1%	164.4 ± 15%
HSC–MDCT	105	0.1	0.60	1.00	67 ± 18%	72 ± 15%	1175 ± 12%	1253 ± 12%	5835 ± 2%	213.7 ± 13%
		0.3	0.60	1.00	67 ± 10%	63 ± 19%	950 ± 12%	1016 ± 11%	4580 ± 2%	221.8 ± 12%
		0.5	0.55	0.93	62 ± 19%	73 ± 25%	620 ± 12%	693 ± 14%	3216 ± 1%	215.5 ± 14%
	112.5	0.1	0.60	1.00	111 ± 15%	112 ± 19%	1300 ± 17%	1427 ± 16%	6326 ± 2%	225.5 ± 14%
		0.3	0.60	0.95	72 ± 12%	91 ± 15%	940 ± 17%	1046 ± 19%	4610 ± 4%	223.7 ± 16%
		0.5	0.55	0.93	56 ± 11%	41 ± 15%	660 ± 7%	692 ± 11%	3388 ± 1%	207.9 ± 8%

Table 6 Results from TPB tests for NSC and HSC mixes.

Concrete	M (kg)	δ_0 (mm)	δ_u (mm)	A (Nmm^2)	$W_{f,nm}$ (Nmm)	$W_{f,m}$ (Nmm)	$W_{f,T}$ (Nmm)	A_{lig} (mm^2)	G_F (N/m)
NSC–TPB	9.7 ± 3%	1.0	1.4	87 ± 12%	62 ± 9%	683 ± 7%	801 ± 8%	5213 ± 2%	153.6 ± 8%
HSC–TPB	11.2 ± 4%	0.7	1.1	89 ± 10%	80 ± 15%	998 ± 9%	1085 ± 12%	5160 ± 1%	209.0 ± 12%

Table 7 Summary of results of G_F for the two concrete mixes NSC and HSC.

Test method	NSC	HSC
TPB	153.6 ± 8%	209.0 ± 12%
MDCT	162.7 ± 15%	218.2 ± 14%

pulling bars stiffness and the necessary compatibility between them and the concrete specimen, which implies slightly higher energy consumption. However, from a statistical point of view, considering the difference between the mean values of each test geometry and concrete and with the obtained coefficient of variation the values obtained in case of MDCT are roughly the same as those obtained in case of TPB and the estimation of G_F, according to the proposed Modified Disk-Shaped Compact Tension test method, is considered to be reliable.

7. Conclusions

The principal conclusions derived from this work are the following:

– Enforced bending of the pulling bars as the crack opens, due to the bar stiffness and the necessary compatibility between the latter and the concrete, influences the stress

distribution along the specimen ligament. As a result, an affected course is noticed at the upper tail of the *P-COD* curve, i.e. at the end of the test. However, in the remaining zones of the curve, in particular till the immediate post-peak part, this effect is negligible and the specimen behavior is entirely satisfactory.

– The affected part of the curve course is amended by using a similar procedure to that proposed by Guinea et al., which provides a size-independent specific fracture energy of concrete, G_F, assessed and compared with that resulting from well validated TPB tests for the same concrete. The results prove that the MDCT test provide reliable results within the range of variation of those for the TPB test, at least for the specimen sizes considered in this work.
– Future work is envisaged to define analytically the correction of the *P-COD* curve at the end of the test as a function of the interaction between steel bar and specimen COD.

Acknowledgments

Authors would like to acknowledge the partial financial supports from the following research projects: BIA2013-48352-P (Ministry of Economy and Competitiveness of Spain), SV-PA-11-012 (Department of Education and Sciences of the Asturian Regional Government) and 16-18702S (Czech science foundation).

Open Access

References

Abdalla, H. M., & Karihaloo, B. L. (2003). Determination of size-independent specific fracture energy of concrete from three-point bend and wedge splitting tests. *Magazine of Concrete Research, 55*(2), 133–141.

Abou El-Mal, H. S. S., Sherbini, A. S., & Sallam, H. E. M. (2015). Mode II fracture toughness of hybrid FRCs. *International Journal of Concrete Structures and Materials, 9*(4), 475–486. doi:10.1007/s40069-015-0117-4.

Amirkhanian, A., Spring, D., Roesler, J., Park, K., & Paulino, G. (2011). Disk-Shaped Compact Tension Test for Plain Concrete. In *Transportation and Development Institute Congress 2011* (pp. 688–698). American Society of Civil Engineers. doi:10.1061/41167(398)66

Amirkhanian, A., Spring, D., Roesler, J., & Paulino, G. (2016). Forward and inverse analysis of concrete fracture using the disk-shaped compact tension test. *ASTM Journal of Testing and Evaluation, 44,* 625–634.

Bazant, Z. P. (1996). Analysis of work-of-fracture method for measuring fracture energy of concrete. *Journal of Engineering Mechanics, ASCE, 122*(2), 138–144.

Bazant, Z. P., & Kazemi, M. T. (1991). Size dependence of concrete fracture energy determined by RILEM work-of-fracture method. *International Journal of Fracture, 51,* 121–138.

Bruhwiler, E., & Wittmann, F. H. (1990). The wedge splitting test: A method of performing stable fracture mechanics tests. *Engineering Fracture Mechanics, 35*(1–3), 117–125.

Cifuentes, H., Alcalde, M., & Medina, F. (2013a). Measuring the size-independent fracture energy of concrete. *Strain, 49*(1), 54–59.

Cifuentes, H., García, F., Maeso, O., & Medina, F. (2013b). Influence of the properties of polypropylene fibres on the fracture behaviour of low-, normal- and high-strength FRC. *Construction and Building Materials, 45,* 130–137.

Cifuentes, H., & Karihaloo, B. L. (2013). Determination of size-independent specific fracture energy of normal- and high-strength self-compacting concrete from wedge splitting tests. *Construction and Building Materials, 48,* 548–553.

De Wilder, K., De Roeck, G., & Vandewalle, L. (2016). The use of advanced optical measurement methods for the mechanical analysis of shear deficient prestressed concrete members. *International Journal of Concrete Structures and Materials, 10*(2), 189–203. doi:10.1007/s40069-016-0135-x.

Elices, M., Guinea, G. V., & Planas, J. (1992). Measurement of the fracture energy using three-point bend tests: Part 3—Influence of cutting the P-d tail. *Materials and Structures, 25,* 327–334.

Gopalaratnam, V. S., & Shah, S. P. (1987). SP105-01 Failure mechanisms and fracture of fiber reinforced concrete. *ACI Special Publication, 105,* 1–26.

Guinea, G. V., Planas, J., & Elices, M. (1992). Measurement of the fracture energy using three-point bend tests: Part 1—Influence of experimental procedures. *Materials and Structures, 25*(4), 212–218.

Harkouss, R. H., & Hamad, B. S. (2015). Performance of high strength self-compacting concrete beams under different modes of failure. *International Journal of Concrete Structures and Materials, 9*(1), 69–88. doi:10.1007/s40069-014-0088-x.

Hillerborg, A., Modéer, M., & Petersson, P. E. (1976). Analysis of crack formation and crack growth in concrete by means of fracture mechanics and finite elements. *Cement and Concrete Research, 6,* 773–782.

Hu, X. Z., & Wittmann, F. H. (1992). Fracture energy and fracture process zone. *Materials and Structures, 25*(6), 319–326.

Issa, M., Issa, M., Islam, M., & Chudnovsky, A. (2000). Size effects in concrete fracture—Part II: Analysis of test results. *International Journal of Fracture, 102*(1), 25–42. doi:10.1023/A:1007677705861.

Karihaloo, B. L. (1995). *Fracture mechanics and structural concrete*. USA: Longman Scientific and Technical Publishers.

Karihaloo, B. L., Abdalla, H. M., & Imjai, T. (2003). A simple method for determining the true specific fracture energy of concrete. *Magazine of Concrete Research, 55*(5), 471–481.

Kim, M., Buttlar, W., Baek, J., & Al-Qadi, I. (2009). Field and laboratory evaluation of fracture resistance of Illinois hot-mix asphalt overlay mixtures. *Transportation Research Record: Journal of the Transportation Research Board, 2127,* 146–154. doi:10.3141/2127-17.

Korte, S., Boel, V., De Corte, W., & De Schutter, G. (2014). Static and fatigue fracture mechanics properties of self-compacting concrete using three-point bending tests and wedge-splitting tests. *Construction and Building Materials, 57,* 1–8. doi:10.1016/j.conbuildmat.2014.01.090.

Kwon, S., Zhao, Z., & Shah, S. (2008). Effect of specimen size on fracture energy and softening curve of concrete: Part II. Inverse analysis and softening curve. *Cement and Concrete Research, 38*(8–9), 1061–1069. doi:10.1016/j.cemconres.2008.03.014.

Lee, J., & Lopez, M. M. (2014). An experimental study on fracture energy of plain concrete. *International Journal of Concrete Structures and Materials, 8*(2), 129–139. doi:10.1007/s40069-014-0068-1.

Linsbauer, H. N., & Tschegg, E. K. (1986). Fracture energy determination of concrete with cube-shaped specimens. *Zement und Beton, 31,* 38–40.

Merta, I., & Tschegg, E. K. (2013). Fracture energy of natural fibre reinforced concrete. *Construction and Building Materials, 40,* 991–997. doi:10.1016/j.conbuildmat.2012.11.060.

Muralidhara, S., Raghu Prasad, B. K., Karihaloo, B. L., & Singh, R. K. (2011). Size-independent fracture energy in plain concrete beams using tri-linear model. *Construction and Building Materials, 25*(7), 3051–3058. doi:10.1016/j.conbuildmat.2011.01.003.

Nam, I. W., & Lee, H. K. (2015). Image analysis and DC conductivity measurement for the evaluation of carbon nanotube distribution in cement matrix. *International Journal of Concrete Structures and Materials, 9*(4), 427–438. doi:10.1007/s40069-015-0121-8.

Nieto, B., Lozano, M., & Seitl, S. (2014). Determining fracture energy parameters of concrete from the modified compact tension test. *Frattura ed Integrità Strutturale, 30,* 383–393. doi:10.3221/IGF-ESIS.30.46.

Pandey, S. R., Kumar, S., & Srivastava, A. K. L. (2016). Determination of double-K fracture parameters of concrete using split-tension cube: A revised procedure. *International Journal of Concrete Structures and Materials*. doi:10.1007/s40069-016-0139-6.

Pinho, S. T., Robinson, P., & Iannucci, L. (2006). Fracture toughness of the tensile and compressive fibre failure modes in laminated composites. *Composites Science and Technology, 66*(13), 2069–2079. doi:10.1016/j.compscitech.2005.12.023.

Planas, J., Elices, M., & Guinea, G. V. (1992). Measurement of the fracture energy using three-point bend tests: Part 2—Influence of bulk energy dissipation. *Materials and Structures, 25,* 305–312.

RILEM. (1985). TCM-85: Determination of the fracture energy of mortar and concrete by means of three-point bend tests on notched beams. *Materials and Structures, 18*(106), 287–290.

RILEM. (2004). TC QFS: "Quasibrittle fracture scaling and size effect"- Final report. *Materials and Structures, 37*(8), 547–568.

RILEM. (2007). TC 187-SOC: Experimental determination of the stress-crack opening curve for concrete in tension. *Final Report of RILEM Technical Committee*.

Shah, S. G., & Kishen, J. M. C. (2011). Fracture properties of concrete-concrete interfaces using digital image correlation. *Experimental Mechanics, 51*(3), 303–313. doi:10.1007/s11340-010-9358-y.

Van Mier, J. G. M. (1991). Mode I fracture of concrete: Discontinuous crack growth and crack interface grain bridging. *Cement and Concrete Research, 21*(1), 1–15. doi:10.1016/0008-8846(91)90025-D.

Veselý, V., Routil, L., & Seitl, S. (2011). Wedge-splitting test-determination of minimal starting notch length for various cement based composites part I: Cohesive crack modelling. *Key Engineering Materials, 452–453,* 77–80.

Vydra, V., Trtík, K., & Vodák, F. (2012). Size independent fracture energy of concrete. *Construction and Building Materials, 26*(1), 357–361.

Wagnoner, M. P., Buttlar, W. G., & Paulino, G. H. (2005). Disk-shaped compact tension test for asphalt concrete fracture. *Experimental Mechanics, 45*(3), 270–277. doi:10.1007/BF02427951.

Wagoner, M., Buttlar, W., Paulino, G., & Blankenship, P. (2006). Laboratory testing suite for characterization of asphalt concrete mixtures obtained from field cores. *Asphalt Paving Technology, 75,* 815–852.

Wittmann, F. H., Rokugo, K., Brühwiler, E., Mihashi, H., & Simonin, P. (1988). Fracture energy and strain softening of concrete as determined by means of compact tension specimens. *Materials and Structures, 21,* 21–32.

Zofka, A., & Braham, A. (2009). Comparison of low-temperature field performance and laboratory testing of 10 test sections in the Midwestern United States. *Transportation Research Record: Journal of the Transportation Research Board, 2127,* 107–114. doi:10.3141/2127-13.